V Kvon et al.

# High re-deposition ratio of metals under high-flux plasma sputtering in Magnum-PSI

# High re-deposition ratio of metals under high-flux plasma sputtering in Magnum-PSI

**V. Kvon[1], E. Zoethout[1], P. Rindt[2], W.M. Arnoldbik[1], J.W. Genuit[1], S. Camp[2], J. Wang[1, 3] and T. W. Morgan[1]**

[1]*DIFFER - Dutch Institute for Fundamental Energy Research, De Zaale 20, 5612 AJ Eindhoven, The Netherlands*

[2]*Science and Technology of Nuclear Fusion, Eindhoven University of Technology, 5600 MB Eindhoven, The Netherlands*

[3]*School of Physics and Nuclear Energy Engineering, Beihang University, 37 Xueyuan Road, Haidian District, Beijing 100191, China*

Corresponding author: **t.w.morgan@differ.nl**

**Abstract:** Plasma core contamination by high-Z impurities must be minimized in a fusion power plant. Excessive concentration of impurities in the core can lead to a drop of the output power as well as give rise to MHD instabilities. Experimental studies of erosion under conditions relevant to the high density and high flux ITER/DEMO divertor conditions are, however, scarce. In this paper, the re-deposition ratios of several metals such as copper, molybdenum and tin under a high flux plasma beam in Magnum-PSI are explored. Samples were exposed to particle fluxes of $0.3–8.5\times10^{23}$ m$^{-2}$s$^{-1}$ in argon or helium plasmas with electron temperatures and densities of $0.6–2.1$ eV and $0.3–5.5\times10^{20}$ m$^{-3}$ respectively, and with ion energies of 5-63 eV. After exposures, the samples were analyzed with X-ray photoelectron spectroscopy, which showed a radial distribution of Mo from the clamping process as the main deposited impurity. Rutherford Backscattering Spectroscopy was then used to quantitatively determine the deposited amount of Mo. Taking this into account two independent techniques were used to measure the net erosion rate: mass loss measured by mass balance after exposures and the mass gain on the quartz crystal microbalance during exposures. Both demonstrated a high level of consistency. Based on these results the calculated re-deposition ratio is >99.8% in the highest flux cases. It was found that the re-deposition ratio strongly scales upwards as a function of particle flux and density. Line emission ratios determined via optical emission spectroscopy also supported these observations. Plasma entrainment of sputtered neutrals is proposed to be the dominant cause of such a high re-deposition rate and calculated mean free paths lengths are closely correlated with the net loss rate, giving good predictions of the observed re-deposition ratios. As similar plasma conditions are expected in ITER and DEMO at the divertor strike points these results indicate that high gross erosion rates could be acceptable at these positions, which could relax divertor design and control requirements and would be particularly beneficial for high-evaporation materials such as liquid metals in future fusion reactors.

**Keywords:** *re-deposition, high-flux plasma, impurities, sputtering, linear plasma devices.*

## 1. Introduction

Plasma material interaction remains a fundamental challenge on the way to the successful implementation of fusion power. Excessive core plasma contamination by erosion and inward transport of impurities from plasma facing components (PFCs) will lead to an undesirable reduction in fusion power, and therefore provides an upper limit on the net impurity flux from the wall materials entering the core plasma. A high re-deposition rate of eroded material can minimize core impurities and increase the lifetime of a PFC by reducing the net erosion rate. Such a situation is more likely to occur when mean free paths are small in relation to the scale size of the divertor, i.e. when the plasma and wall enter the strongly coupled regime, which is what is expected in detached conditions at the ITER divertor size scale [1]. Particularly in the case where evaporation is the dominant erosion mechanism, which is the case for liquid metals such as lithium (Li) and tin (Sn), a high re-deposition rate could also increase the temperature window for operation of such a PFC [2].

Until now there was rather limited data on the re-deposition rate measurement under ITER/DEMO divertor relevant plasma fluxes [1][4][5] where very high incoming particle fluxes and low ion and electron temperatures are anticipated. Recent work indicated that under Ar plasma exposure liquid Sn test targets investigated in Pilot-PSI [6] exhibited an implicit re-deposition rate of 98-99.8% [8], while other studies in Pilot-PSI or Magnum-PSI have also indicated a high re-deposition rate under high flux plasma [7] [9]. In this paper, dedicated studies have been carried out to investigate the re-deposition ratio of several different metals (copper (Cu), molybdenum (Mo) and tin (Sn)) under high flux plasma exposure in Magnum-PSI [10][11][12]. Sn is considered as a prospective material for use in a liquid metal divertor in DEMO [13][14] and, as stated above, is a material where a high re-deposition rate was apparent. Cu was chosen as a metal with a relatively high sputtering yield and which had the advantage that it can visually indicate the presence of many impurities on its surface, while Mo was used as a reference where sputtering should be close to negligible.

The experimental conditions and samples are described in Section 2 and 3 respectively. The methodology used for calculations and measurements is given in Section 4. Results are given in Section 5 and are divided into 3 subsections following the notation given in Table 1, while Section 6 discusses the results and process that can lead to the observed re-deposition ratios. Lastly, the interpretation and implications of the obtained measurements are outlined in Section 7.

## 2. Experimental setup and diagnostics

Experiments were conducted in the linear plasma machine Magnum-PSI. The machine was designed to obtain ITER divertor-like and above ITER divertor-like conditions to test materials under high flux, low electron temperature plasma exposure [1][11][12]. With a recently installed superconducting magnet Magnum-PSI can reach steady state magnetic field up to 2.5 T, electron temperatures ~6 eV and deliver a high flux of up to ~$1 \times 10^{25}$ m$^{-2}$ s$^{-1}$ plasma at beam centre to a target surface. In the experiments reported here the magnetic field was varied between $B = 0.2$–$0.8$ T, peak fluxes at beam centre were $\Gamma = 0.3 \times 10^{23}$–$8.5 \times 10^{23}$ m$^{-2}$ s$^{-1}$ and the duration of a single exposure lay typically in the range $t = 20$–$40$ s. Experiments were performed in argon (Ar) and helium (He) plasmas. These conditions were chosen to limit the surface temperature of the target materials to a regime where evaporation was negligible.

The spectrum composition was monitored using by optical emission spectroscopy (OES), with two spectrometers (Avantes AvaSpec-2048-USM2-RM): one in the range of 299-590 nm viewing close to normally at the target and one in the range 378-950 nm viewing tangentially in front of the target at the Thomson scattering position, approximately 3 cm from the target surface. Thomson scattering (TS) was used to measure electron temperature ($T_e$) and electron density ($n_e$) near the target [16] at the same axial position as the tangential OES view. Parameters of the discharge in the plasma centre were: $T_e = 0.6$–$2.1$ eV and $n_e = 3.0 \times 10^{19}$–$5.5 \times 10^{20}$ m$^{-3}$ dependent on the field and the target bias. Example radial profiles of $T_e$ and $n_e$ are shown in figure 1.

The targets were biased at -50 V, -30 V or kept at floating potential. For the argon cases, the measured floating potential was slightly positive relative to ground (~5V) while for He it was close to zero. This was taken into account when determining the ion energy for sputtering. The sample temperature was monitored by IR camera (FLIR SC7500MB, 4.5 kHz) and direct temperature measurements were performed using an N-type

thermocouple, installed inside each sample in close contact with the plasma exposed surface. A tangential view of the plasma region in front of the samples was observed by fast visible camera (Phantom V12). In addition a quartz crystal microbalance (QCM), (Inficon front load single sensor/STM-2 PN 074-613-P1D), was installed in the vacuum chamber near the target to accumulate sputtered particles. It was positioned at an angle of 45° with respect to the target normal and at a distance of 25±2 cm. The QCM crystal exposed surface was 8.25 mm in diameter.
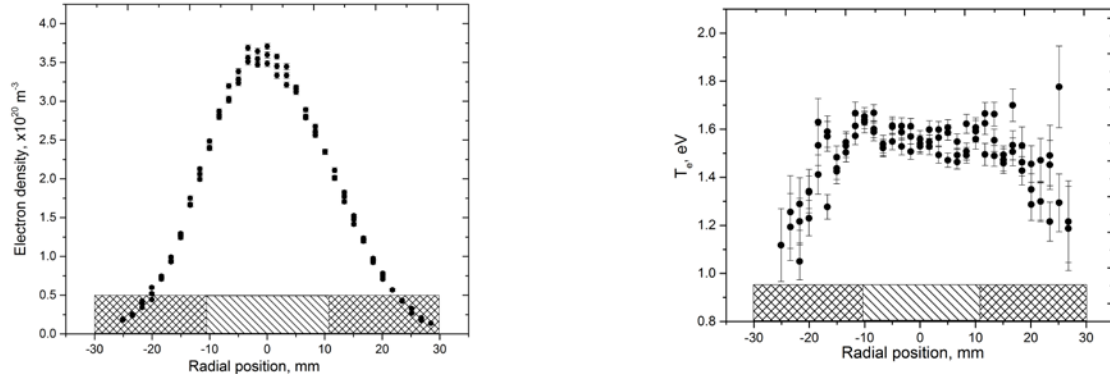


**Figure 1: Thomson scattering measurements of electron density (left) and electron temperature (right) profiles along the sample surface: B=0.6 T, bias -50 V. The area of a sample (dashed) and the area of a clamping ring (crossed) exposed to the plasma beam are shown to illustrate the beam dimensions relative to the samples.**

## 3. Samples

Samples were produced from molybdenum (99.97 % purity), copper (E-Cu57, ≥99.90% purity) and tin (99.99+% high purity Goodfellow ltd.). Copper (Cu) and molybdenum (Mo) samples were manufactured as cups with 1 mm base thickness and 4 mm rim thickness, with outer diameter of 30 mm and the inner diameter of 22 mm (figure 2). This geometry was chosen to minimize the sample thickness in the centre to reduce surface temperature while fitting in the 4 mm deep, 5 mm thick Mo clamping ring. The surface roughness was analyzed with an optical microscope (Zeiss Imager Z2M), giving the horizontal roughness as 50-300 μm. Vertical roughness was resolved with a profilometer (Bruker DektakXT) and was measured to be ~7μm. Tin (Sn) samples were re-produced as in our previous paper [8]. In short, a 4 mm thick, 3 mm deep Mo cup was filled with Mo mesh (0.2 and 0.44 mm diameter pore sizes) and then impregnated with Sn. The thickness of Sn samples was 4 mm and the inner diameter was 22 mm, identical to the Mo and Cu samples. All samples were clamped by a Mo clamping ring of 5 mm thickness and 60 mm in diameter. The region where the sample (dashed) and the clamping ring (crossed) is exposed to the plasma beam is indicated in figure 1.

After plasma exposure, the samples were analyzed by X-ray photoelectron spectroscopy (XPS). The composition of the top surface was studied in a vacuum environment of $1 \times 10^{-8}$ mbar. Monochromatic Al-K$_{\alpha}$ radiation was used to investigate the surface. For quantification of the measured XPS spectra, element specific peaks are identified. The peak areas of the identified elements are determined and corrected for the element specific sensitivity factors from the Scofield library [17]. The element specific normalized surface area (hereafter simply called normalized intensity) can be used as a measure of the atomic concentration of the observed elements. XPS scans were performed radially from the centre of the sample to the edge at a footprint diameter of approximately 0.5 mm. This resulted in a radial profile of the chemical composition of the surface (approximately the top 10 nm).

After the experiments it was found that Mo, sputtered from the clamping ring, was deposited on the samples. To quantify this amount the samples were also analyzed using Rutherford Backscattering Spectroscopy (RBS) using the Ion Beam Analysis Station at DIFFER. A 2.0 MeV $^{4}$He beam generated by a High Voltage Engineering Singletron accelerator was used with two detectors at 170° and 150° scattering angle. The 2×2 mm beam spot was scanned across the surface diameter in 2 mm steps. The RBS spectra were used to determine the quantitative amount of deposited Mo with a 1-5 % accuracy as a function of target radius. For the Sn

samples, determination of the Mo amounts was not possible in a straightforward manner, while distinguishing the deposited Mo was naturally impossible for the Mo sample. Expected deposition masses of Mo are therefore estimated in these cases by extrapolation from the Cu exposures as the Mo clamping ring was identical in all cases.



**Figure 2: Copper sample photograph and optical microscope images of its surface.**

## 4. Methodology

*4.1 Experimental conditions*

The experimental series were divided into three groups. The list of samples and exposure conditions is given in Table 1:

- The first group consisted of 4 copper samples and was devoted to the study of the flux influence: during their plasma exposure the ion energy was kept approximately constant, but the magnetic field i.e. the incoming ion flux, varied.
- The second group consisted of three copper samples and was devoted to study the influence of the incoming ion energy. During the plasma exposure of these 3 samples the magnetic field was fixed at 0.4 T, but the bias was different per each sample.
- The third group consisted of two tin samples, one copper and one molybdenum sample. The aim in this experimental series was to investigate re-deposition with different plasma species and target element.

| Group number | Target designation and material | $t$ [s] | $E_{ion}$ [eV] | $B$ [T] | $\Gamma_i$ [$\times 10^{23}\,m^{-2}\,s^{-1}$] | $T_e$ [eV] | $n_e$ [$\times 10^{20}\,m^{-3}$] | $L_{plasma}$ [mm] |
|---|---|---|---|---|---|---|---|---|
| | Cu 1 | 30 | 58 | **0.2** | 0.3 | 0.6 | 0.3 | 38 |
| **1** | Cu 2 | 40 | 61 | **0.4** | 1.1 | 1.2 | 0.8 | 33 |
| | Cu 3 | 20 | 63 | **0.6** | 5.7 | 1.5 | 3.7 | 26 |
| | Cu 4 | 30 | 63 | **0.8** | 8.5 | 1.5 | 5.5 | 24 |
| | Cu 5 | 30 | **5** | 0.4 | 3.0 | 0.9 | 2.5 | 33 |
| **2** | Cu 6 | 30 | **41** | 0.4 | 1.7 | 1.3 | 1.2 | 33 |
| | Cu 2 | 40 | **61** | 0.4 | 1.1 | 1.2 | 0.8 | 33 |
| | **Cu 8 (He plasma)** | 40 | 57 | 0.4 | 1.7 | 2.1 | 0.3 | 22 |
| **3** | **Mo 1** | 170 | 38 | 0.2 | 0.3 | 0.7 | 0.3 | 38 |
| | **Sn 1** | 60 | 38 | 0.2 | 0.3 | 0.7 | 0.3 | 38 |
| | **Sn 2** | 40 | 41 | 0.4 | 1.7 | 1.3 | 1.2 | 33 |

The total incoming flux of ions ($\Gamma_i$) was calculated based on TS measurements of the electron density and temperature [15]:

$$\Gamma_i \approx \frac{1}{2}n_i\sqrt{\frac{k(T_e + \gamma T_i)}{m_i}} \qquad (1)$$

where $n_i$ is the ion density, $k$ is the Boltzmann constant, $T_e$ and $T_i$ are electron and ion temperatures, respectively, $\gamma$ is the adiabatic constant, which is taken to be 5/3, and $m_i$ is the ion mass. We assume that $T_e \approx T_i$ and $n_i \approx n_e$ [16].

*4.2 Temperature monitoring*

Under a high flux of energetic ions, excessive heating of the target can act as an additional loss term due to evaporation. This can lead to significant source of error in determining re-deposition ratio due to the requirement to accurately know the surface temperature distribution. Therefore, during experiments it was important to monitor the sample temperature to ensure temperatures were kept at levels where evaporation is negligible. This was done by minimizing the target thickness to 1 mm for Cu and Mo samples and installing a thermocouple inside of them to monitor this. This design and arrangements were tested in a preliminary set of experiments with the same discharge settings (see Table 1) prior to the actual experimental series.
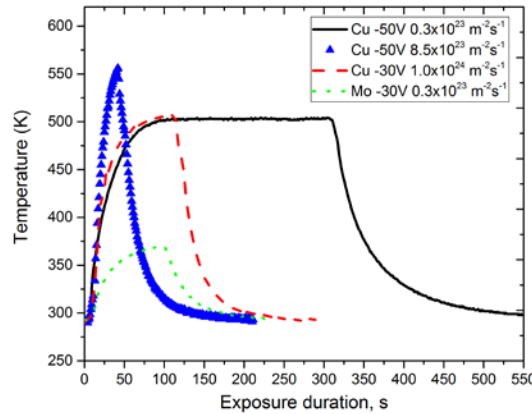


Figure 3: Example Cu and Mo sample temperature evolution during long plasma exposures.

Cu and Mo samples were exposed to extended discharges to obtain a time period when the temperature of a sample reaches a plateau. As can be seen in figure 3, Cu and Mo samples reach a stable temperature not higher than 570 K at the highest fluxes. At these temperatures, the impact of evaporation on mass loss of Cu and Mo targets is negligible [18]. Thermocouples were not inserted in the Sn targets; however, during the experiments it was observed that the Sn did not melt, which indicates the temperature remained below 505 K, where evaporation is also negligible.

*4.3 Re-deposition ratio determination*

To measure the re-deposition ratio we utilized two methods. The first was to measure the mass loss of each sample ($\Delta m_{loss}^m$) with a microbalance (Metler Toledo NewClassic MF MS105DU) after the plasma exposure

5

and compare it with the expected mass loss ($\Delta m_{\text{loss}}^{\text{e}}$). The weighing of the samples was carried out at least 5 times per sample prior to the plasma exposure and 5 times after the experiment, with a statistical error evaluation for every measurement series. Some Mo was deposited on most samples from the sputtering of the clamping rings. The mass gain $\Delta m_{\text{gain,Mo}}^{\text{m}}$ due to this was measured via RBS on each sample individually and taken into account in determining the mass loss of the target material.

The expected mass loss was calculated as the sputtering process in the absence of any re-deposition. The expected mass loss due to sputtering as a function of radial position ($r$) was calculated using [19]:

$$\Delta m_{\text{loss}}^{\text{e}} = \int_0^{r_{\max}} 2\pi r \, Y(E_{\text{ion}}, i, z) * M_{\text{z}} * \Gamma_{\text{i}}(r) t \, \mathrm{d}r \qquad (2)$$

where $Y$ is the sputtering yield, which is a function of the ion energy ($E_{\text{ion}}$), the ion species ($i$) and target species ($z$); $M_{\text{z}}$ is the target atomic mass and $t$ is the duration of the exposure. This function was calculated in MATLAB based on TS profile measurements along the sample surface. The sputtering yield for each metal was taken from [19]. To choose the appropriate ion energy and the subsequent sputtering yield we determined the ion energy due to biasing and the sheath acceleration with the formula: $E_{\text{ion}} = eV_{\text{bias}} - eV_{\text{f}} + 5.5kT_{\text{e}}$ where $e$ is the electron charge, $V_{\text{bias}}$ is the bias voltage and $V_{\text{f}}$ is the floating potential (which was measured for each discharge condition). Note that for the argon plasmas the measured floating potential was typically around +5 V while for He it was close to zero, typically giving an ion energy slightly higher than the bias voltages used. Given the uncertainty in the ion energy and the fact that the sputtering yields are relatively close to threshold we assign an error bar of 50% to the determined sputtering yield, as discussed in [8]. To take into account the Mo mesh in the Sn samples we accounted for the open area values claimed by its manufacturer. Therefore, Sn was assumed to be sputtered only from the areas between the pores. The impact of Mo mesh in the mass loss was adjusted accordingly by then taking sputter rates for Mo. Again this gives a conservative estimate for the expected mass loss as the mesh was observed to be wetted by the Sn, meaning that in the sample the plasma facing material is therefore expected to be only Sn [13]. The re-deposition ratio from mass loss is therefore calculated as $R_{\text{loss}} = 1 - (\Delta m_{\text{loss}}^{\text{m}} + \Delta m_{\text{gain,Mo}}^{\text{m}})/\Delta m_{\text{loss}}^{\text{e}}$.

The second method was to measure the mass gain on the QCM ($\Delta m_{\text{gain}}^{\text{m}}$) due to the deposition of sputtered material and compare it with the expected mass that should be deposited in the absence of any re-deposition ($\Delta m_{\text{gain}}^{\text{e}}$). The measured mass gain was determined from the frequency change of the crystal using both the Sauerbrey equation [20] and the Z-match method [21], both of which agreed within 1%. The error bar arises from the standard deviation of the statistical noise in the measured signal. RBS measurements of the QCM crystal used gave complicated results due to the complex structure of the deposited layers and the fact that the silver coating on the crystal is higher in mass than the deposited elements. Therefore, a reasonable estimate of the contribution from the clamping ring is not possible. To give the smallest possible re-deposition ratio (i.e. the most conservative assumption) we assume that all deposited material is solely due to the target element sputter deposition and that the clamping ring contribution is negligible.

In this case, we determine the expected mass gain as $\Delta m_{\text{gain}}^{\text{e}} = \Delta m_{\text{loss}}^{\text{e}} \Omega$, where $\Omega$ is the solid angle subtended by the QCM. To evaluate the fraction of total sputtered atoms that theoretically can be deposited on the QCM we assumed that sputtered atoms are isotropically distributed in the solid angle of $2\pi$ after sputtering. This assumption can be justified taking into account that the sample surface is rather rough (see Figure 2) and therefore any preferential direction of sputtered atoms should be averaged by the morphology of the surface. The re-deposition ratio from mass gain is therefore calculated as $R_{\text{gain}} = 1 - \Delta m_{\text{gain}}^{\text{m}}/\Delta m_{\text{gain}}^{\text{e}}$.

## 5. Experimental results

6

We structure our experimental results as follows: at first, we show XPS measurements and photographs for each group of samples (see Section 3 and Table 1) as well as the RBS analysis. Afterwards we analyzed the mass loss of each sample and the mass gain on the QCM during this sample exposure then compared them with expected mass loss or gain without re-deposition to determine the re-deposition ratio. In addition, as the targets' material is sputtered we observed emission radiation from the sputtered atoms. By comparing the ratio of emission at the target surface with that at the TS position complementary information about re-deposition was also determined.

*5.1 Group 1: Influence of flux on the sample mass measurements*

Group 1 consisted of 4 copper samples where the ion energy of the pure Ar plasma was held approximately constant at 58-63 eV. The magnetic field and thus the incoming flux of ions was different for each sample (Table 1: Group 1). As mentioned above, samples were clamped by a Mo clamping ring, a part of which was exposed to the plasma beam (Figure 1). In this area, the ion flux was much lower than in the center of the beam, but still could lead to Mo sputtering and re-deposition due to the same bias of the clamping ring as the target. Indeed, after plasma exposures all samples demonstrated Mo deposition on their surface, which is clearly visible due to the colour difference between Mo and Cu. The gradual increase of Mo re-deposition has been observed optically (as a silver-grey metallic layer) and confirmed with XPS measurements (Figures 4 and 5) and RBS measurements (Figure 5.1). The XPS results in all cases show that Mo is the pre-dominant impurity deposited. C and O are also present, but are presumed to be from the atmospheric exposure and their contribution to the target mass change is neglected.
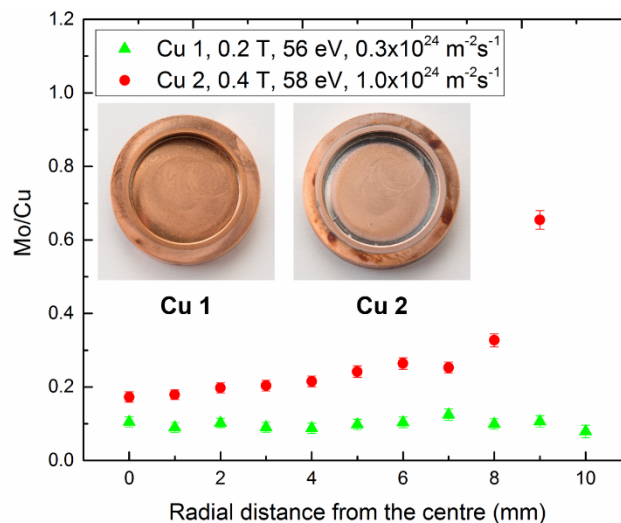


**Figure 4: Normalized intensity ratio of Mo and Cu of samples Cu 1 and Cu 2 and their photographs after plasma exposure.**

For lower fields of 0.2 T and 0.4 T, with fluxes $0.3 \times 10^{23}$ and $1.0 \times 10^{23}$ $m^{-2}s^{-1}$ respectively, XPS showed a relatively small ratio <1 of Mo to Cu (Figure 4). For the sample Cu 1 the incoming flux was not dense enough to have a significant re-deposition of Mo. In contrast, Cu 2 demonstrated a higher ratio of Mo to Cu, which radially increases towards the periphery of the sample, which correlates with the visibly observed silver ring of Mo. This indicates that at lower plasma beam fluxes the Mo re-deposition ratio is low although it clearly occurs. Further, the fact that the re-deposition is strongly concentrated towards the edge of the sample implies that at the edges re-deposition is at least partially due to line-of-sight deposition, mean free paths are small, and/or that the edges are net deposition regions for the Mo.
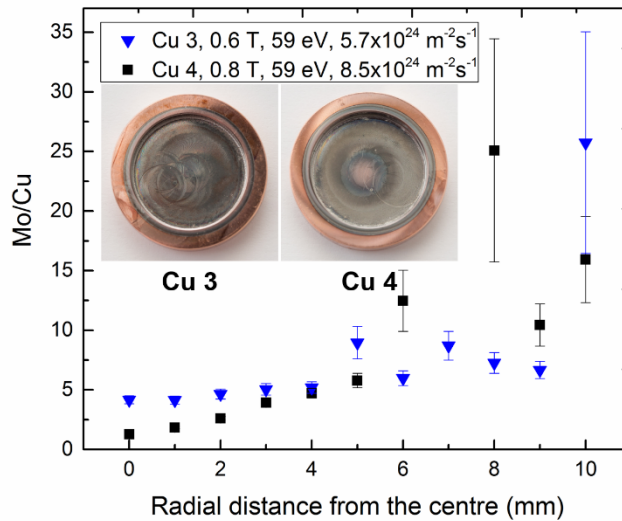
**Figure 5: Normalized intensity ratio of Mo and Cu of samples Cu 3 and Cu 4 and their photographs after plasma exposure.**

1

2    For higher fields of 0.6 T and 0.8 T, with fluxes $5.7 \times 10^{23}$ and $8.5 \times 10^{23}$ $m^{-2}s^{-1}$ respectively, XPS showed much

3    high ratios $\gg 1$ of Mo to Cu (Figure 5) than in the previous case. This indicates that at higher plasma beam

4    fluxes the re-deposition is significant. It appears that not only Cu, but also Mo sputtered from the clamping ring

5    is re-deposited back on the sample surface.

6
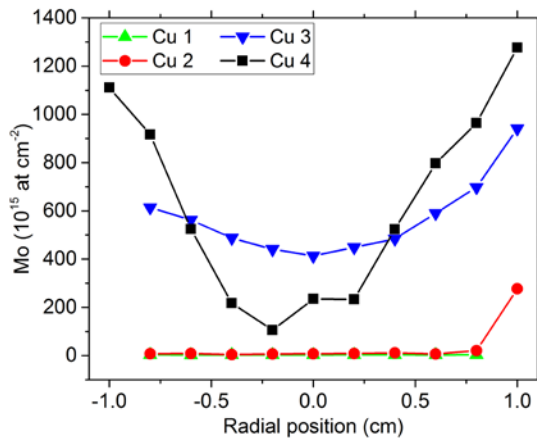


**Figure 5.1: Areal density of deposited Mo measured by RBS as a function of radial position for samples Cu1-Cu4.**

7

8

9    The RBS analysis confirms the thin deposition layer of Mo increases with increasing flux. The deposition

10   profiles for these four samples are shown in figure 5.1. These agree very well with the qualitative analysis from

11   the XPS.

12
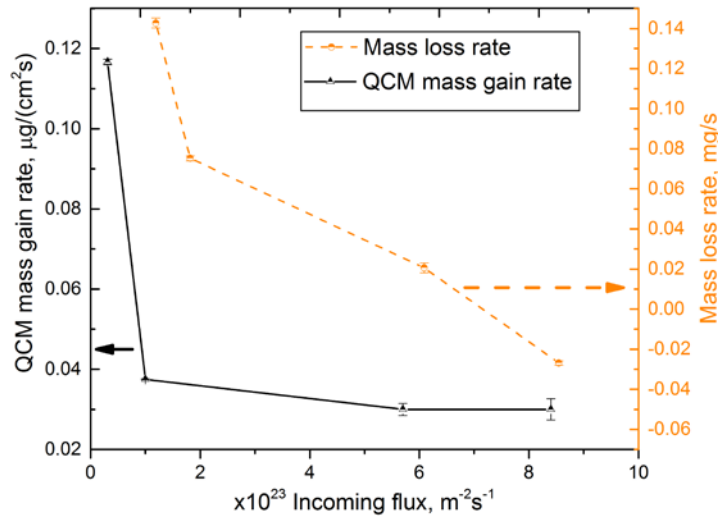
**Figure 6: QCM mass gain rate (solid black line) and mass loss rate (orange dashed line) dependences on the incoming flux magnitude.**

1
2  The mass loss rate and mass gain rate on QCM showed consistent results (Figure 6). Qualitatively, the generally
3  decreasing trend in both measurements can be understood as a dependence on the flux magnitude. As the
4  incoming flux becomes larger more particles are not only sputtered, but also are re-deposited back. This effect
5  must increase with flux as without this the expected mass loss rate would be expected to increase rather than
6  decrease as a function of flux.
7  The mass gain rate on the QCM can be understood as being related to the net loss rate from the local target
8  region. This also decreases with a larger flux, which implies that despite the greater sputtering rate (which
9  would be expected to produce a higher rate as a function of flux) the large re-deposition ratio means overall
10 fewer atoms can reach the QCM crystal. The physical phenomena, which can account for this trend, are
11 discussed in detail in Section 6.
12
13 *5.2 Group 2: Influence of ion energy on the sample mass measurements*
14 The next group of samples was devoted to the investigation of the effect of different ion energies. Group 2
15 consisted of 3 copper samples that were exposed in the same magnetic field of 0.4 T, but at different biases.
16 The plasma contained only Ar species, but the bias, thus the energy of incoming ions, was different per each
17 sample (see Table 1: Group 2).
18 For the floating potential case (Cu 5), both XPS and optical images of the sample did not reveal any Mo
19 presence. In addition, the sample did not have any mass loss ($\Delta m_{loss}^{m}$=-0.04±0.03 mg) after the exposure and
20 no mass gain on QCM ($\Delta m_{gain}^{m}$ = -4 ng/cm$^2$) was observed during the plasma shot. These measurements are
21 consistent with the assumption that no sputtering and therefore no re-deposition occurs at a floating potential.
22 Thus, this can help to ensure that all mass gain or loss observed on the QCM and target is due to the sputtering
23 and re-deposition processes rather than environmental factors from the background gas or impurities from the
24 plasma source or wall.
25 For the negatively biased cases in this experimental series, XPS showed similar ratio between Mo and Cu
26 normalized intensity ratios to the lower field exposure in Group 1 (compare Figures 4 and 7). The images also
27 comply with the XPS measurements. For the lower biased case (Cu 6) the results are very similar to the higher
28 biased case (Cu 2), indicating that biasing rate does not play as strong a role as flux dependence in the overall
29 re-deposition process. The RBS results show that for Cu 6 the deposited layer was around twice as thick
30 ($6.8\times10^{15}$ cm$^{-2}$) as the layer for sample Cu 2 ($3.2\times10^{15}$ cm$^{-2}$), despite the lower ion energy in the former case.
31 This reinforces the conclusion that flux and electron density play the most important role in the re-deposition
32 rate.
33
34
35

**Figure 7: Normalized intensity ratio of Mo and Cu peaks of samples Cu 6 and Cu 2and their photographs after plasma exposure.**
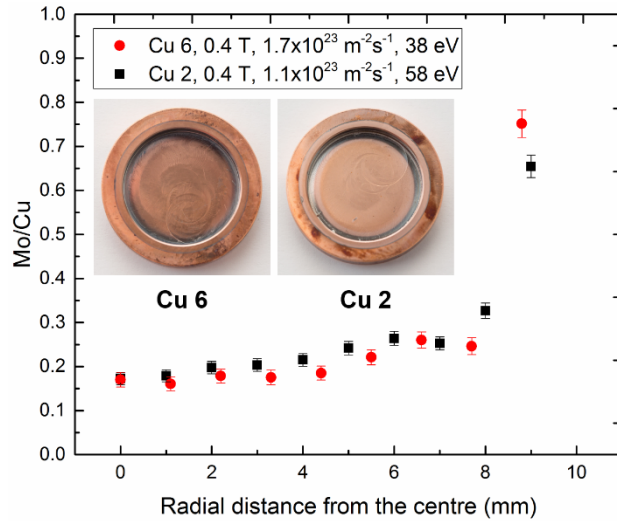
1
2  Mass loss rate and mass gain rate on the QCM again showed good consistency with each other: although the
3  sputtering yield was around 38% that of Cu 2, the flux magnitude was ~65% bigger in the smaller bias case.
4  Therefore, overall we expected the gross yields at -30 V to be 59% those at -50 V. However in total the mass
5  loss rate is around 28% that of Cu 6 and around 34% in terms of mass gain. Therefore, the re-deposition was
6  more prominent at bigger flux with higher density, and consequently the mass loss rate and the mass gain rate
7  on QCM are smaller than expected for the -30 V biased sample relative to the -50 V biased sample (Figure 8).
8
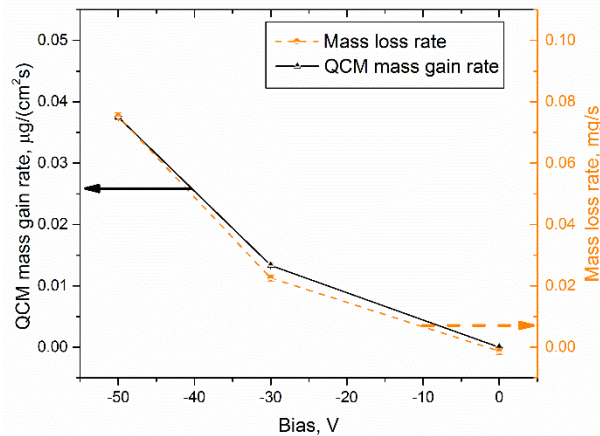


**Figure 8: QCM mass gain rate (solid black line) and mass loss rate (orange dashed line) dependences on the bias magnitude.**

9
10 *5.3 Group 3: Sample mass measurements under different exposure conditions and target materials*
11 Measurements were carried out with the aim of investigating re-deposition using ion and target species
12 combinations other than Ar and Cu: changing gas type from Ar to He (sample Cu 8) while maintaining a Cu
13 target; changing the target material to Mo (sample Mo 1) with Ar plasma, and finally changes the target material
14 to solid tin with Mo mesh embedded (samples Sn 1 and Sn 2) with Ar plasma.
15 For sample Cu 8 the XPS results demonstrated a similar ratio of Mo to Cu as for Ar plasma, which varies from
16 0.7 in the centre up to 1.1 at the edge compared to 0.2-0.6 for Cu 2. The flux in this case was a factor 1.7 higher
17 than for Ar, but this ratio is rather high giving that Mo sputtering should be negligible at such small energies
18 of incoming He ions: the sputtering yield in such a case is very close to threshold with a large uncertainty [19]

10

1    but certainly <$10^{-3}$. This implies that the amount of Mo sputtering must be very small. However, we clearly
2    observed strong discolouration on our sample. The RBS results showed that Mo is present on the sample in
3    amounts consistent with the XPS analysis 72±6 µg in total were deposited. This is negligible compared to the
4    Cu sputtering but sufficient to cause the discolouration. The RBS profile is also peaked in the centre unlike the
5    other cases, indicating that the source of Mo may come from the plasma for this sample. When using He here
6    the voltages between plates in the source are much higher than for Ar, which may mean that Mo inserts in the
7    source were sputtered and deposit on the surface of the sample in this case. The mass loss rate of Cu 8 sample
8    was measured to be 7 µg/s and QCM mass gain rate was 7 ng/(s cm$^2$).
9
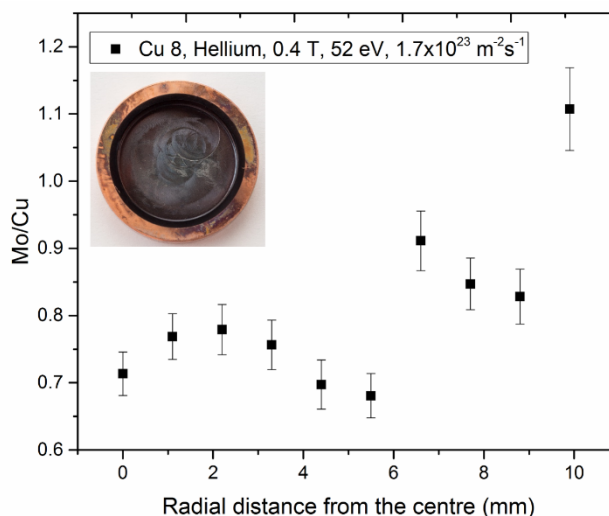


**Figure 9: Normalized intensity ratio of Mo and Cu of Cu 8 sample and it's photograph after helium plasma exposure.**

10
11   Mo sputtering in argon plasma was also investigated, also below or close to sputtering threshold. A Mo sample
12   was exposed to Ar plasma at -30 V bias, 0.2 T with the incoming flux of $0.3 \times 10^{23}$ m$^{-2}$s$^{-1}$. At such conditions,
13   we expected to observe the re-deposition rate to not be very strong, based on the measurements in the previous
14   two groups with same conditions (compare Cu 1 sample). The sputtering threshold of Mo for argon ions with
15   energies ~38 eV is very close to threshold with Y~$5 \times 10^{-4}$ [19]. During Mo sample plasma exposure, we still
16   observed a mass loss of Mo sample, with a small and simultaneous QCM mass gain. The mass loss rate was
17   measured to be 3 µg/s and QCM mass gain rate of 8 ng/(cm$^2$ s) was acquired during the sample exposure.
18   However, the mass changes were so small and the uncertainties in expected mass changes so large that a
19   meaningful determination of the re-deposition ratio was not possible.
20   For the Sn samples no droplets in the discharge were observed on Phantom V12 and FLIR IR cameras, and as
21   stated earlier the temperature was below that required for evaporation. These observations suggest that the
22   target surface erosion was pre-dominantly due to sputtering by the plasma beam. The mass loss rate for the Sn
23   2 sample was measured to be 10 µg/s and QCM detected gain of 6 ng/(cm$^2$ s). For the Sn 1 sample, the plasma
24   flux was smaller and as expected the mass loss rate and QCM mass gain rate were larger than for sample Sn 2
25   due to lower re-deposition rates. The mass loss rate and QCM mass gain rate were measured to be 25 µg/s and
26   was 11 ng/(cm$^2$ s) respectively.
27
28   *5.4 Optical Emission spectroscopy results*
29   OES measurements also suggest an increase of re-deposition with increasing flux. Figure 10 demonstrates the
30   ratio between intensities of Cu II lines, as well as Mo I lines, at two different positions simultaneously: at the
31   target position and at the TS position. The ratio of these intensities was then calculated. Unfortunately only a
32   small wavelength range could be observed in two locations and in this region Mo and Cu spectra are very close
33   together. Therefore our spectrometer could not resolve Mo I lines from Cu II. The lines are strong Mo I lines
34   and weak Cu II lines [23]. However, OES signals during two samples at the same exposure conditions: Cu 6

(Cu and Mo species are present) and Sn 1 (only Mo species no Cu are present), revealed that Cu does have a significant impact on Cu+Mo intensity. In this case it is about 60% of the total intensity. This indicates that the erosion rate of Cu is much higher than Mo, as would be expected, and that Cu is at least partially ionized in the plasma as Cu II is observed. Figure 10 shows the sum of both species lines intensities at different incoming plasma fluxes for the group 1 targets.
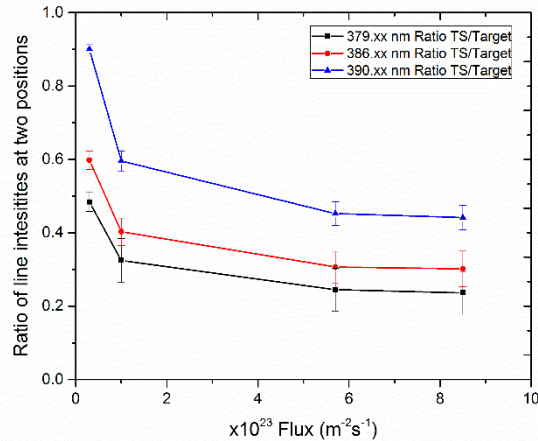


**Figure 10: Ratio of intensity of Cu and Mo lines at the target and TS positions. Numbers indicate wavelengths in nm near which several strong Cu and Mo lines are located (wavelengths from NIST [23]).**

## 6. Discussion

XPS measurements demonstrated a significant presence of Mo on our Cu targets. Therefore, Mo clamping rings which were at the same bias as samples during the exposure, were sputtered and subsequently re-deposited on the target surface. Furthermore, radial XPS spectra showed that there is a radial increase of the Mo to Cu ratio for all measured Cu samples (see Figures 4, 5, 7 and 9). RBS spectra generally support this and show that it increases from the centre to the periphery of a sample (figure 5.1) with the exception of Cu 8. As the clamping ring was placed concentrically on the target's edge, such as that the central inner part of the target with the diameter of 22 mm is fully exposed to the plasma beam (see Figure 2), the rims of the Cu targets were closer to the Mo clamping ring than target's centre, thus Mo atoms that were sputtered and re-deposited would more likely concentrate on the rim side of the Cu sample if the path lengths are much smaller than the size of the target. This tends therefore to support a re-deposition process with a path length of only a few mm.

A general trend of mass loss rate decrease with the increase of the incoming ion flux was measured for all 3 groups, despite the increasing gross sputtering rate with ion flux (Table 2 and figure 11). The mass gain rate on the QCM also follows the same decreasing dependence with increasing flux. It is important to try to identify the mechanism, which can drive this.

Ionized sputtered particles return easily to the surface due to the strong electric field if this occurs in the sheath, or due to entrainment in the plasma outside of that [15][24]. Therefore, electron impact ionization and subsequent re-deposition of ions back to the negatively biased target is considered. However, according to literature the maximum ionization cross-section is $3-4\times10^{-20}$ m$^{-2}$ at ~35 eV for Cu and $4-9\times10^{-20}$ m$^{-2}$ at 40 eV for Mo [25][26][27][28][29], but in our experimental condition the electron temperature was ~1-2 eV, and the cross-sections are many orders smaller. Even considering that the sputtered particles can have energies up to half the surface binding energy ($E_{sb}$) the cross sections for ionization are still very small (Mo has the largest with $E_{sb}$ =6.85 eV [30]). We can conclude that the cross-section for this process in our plasma was $<10^{-22}$ m$^{-2}$ for all ion-neutral combinations. Therefore, due to small electron energy and small magnitude of the corresponding cross-sections (comparing to the next discussed processes), electron-impact ionization is not considered as the most influential.

Second, we consider entrainment [24] of sputtered atoms back to the target surface due to interaction with plasma ions. This is driven by inducing a dipole in the atom due to a nearby charged particle. This phenomenon becomes more and more prominent if the density and subsequently the flux of the incoming ions increases. To

estimate this process we use the cross-section for momentum transfer between ions and atoms at low energies [31]:

$$\sigma_{mt} = \frac{3\sqrt{2}}{16}\pi^{3/2}\left(\frac{4.88\alpha e^2}{\mu}\right)^{1/2}\left[\frac{kT_i}{m_i} + \frac{kT_n}{m_n}\right]^{-1/2} \tag{3}$$

where $\alpha$ is the atom polarizability and $\mu$ the reduced mass. Polarizabilities of Cu, Mo and Sn were taken as an average value from several references to be 15.5 $\text{Å}^3$, 13.6 $\text{Å}^3$ and 5.9 $\text{Å}^3$ [32] respectively. The cross-sections calculated with formula (3) for Ar-Mo and Ar-Cu interactions are ~1-6x$10^{-19}$ $\text{m}^{-2}$, which are an order of magnitude bigger than the maximum ionization cross-sections listed above, which are also valid at energies of tens of eV rather than the current case.

Charge-exchange (CXR) is another process which can lead to particle charging and subsequent ion-ion collisions, which are more efficient to induce entrainment. Typically non-resonant charge transfer such as would be present here is not considered as an important channel, however the fact that weak Cu II emission lines are observed indicates that at least some sputtered copper becomes charged, which as stated above has a low probability due to electron impact ionization. No literature was available for the cross-sections between the species here, however for low energy collisions Hutchinson suggests a formula [33] to estimate the cross sections when a resonance occurs at a particular ion-neutral separation as they approach one another:

$$\sigma_{CXR} \approx 8\pi a_0{}^2 n_n{}^4 Z_i\left[1 + \sqrt{1/Z_i} + 1/4Z_i\right] \tag{4}$$

where $n_n$ is the quantum level of the neutral (taken to be 1, i.e. ground state), and and $Z_i$ the charge of the ion (also taken to be 1). The case applied in [31] is valid for fully ionized ions interacting with neutral hydrogen, therefore this gives only a crude estimate. However, this gives $\sigma_{CXR}$~2.6x$10^{-19}$ $\text{m}^2$, which is energy independent at low energies and thus identical for all our species pairs. Despite the poor approximation, it does indicate that this can still be an important process in this case as it is the same order as the momentum transfer. More accurate data would give a much clearer indication of its significance.

After calculating these cross-sections per each pair of the gas ion and the target metal in our experiments i.e. Ar-Mo, Ar-Cu, He-Cu, He-Mo and Ar-Sn, the mean free path (MFP) is determined as $\lambda_{\text{MFP}} = 1/[(\sigma_{mt} + \sigma_{CXR})n_i]$, where $n_i$ is assumed to be equal $n_e$ which is measured by TS. We can expect the following: the larger the plasma density the smaller the MFP and thus smaller the mass loss rate and QCM mass gain rate. This indicates that the re-deposition ratio should be higher at larger fluxes and larger $n_i$. Table 2 shows calculated MFP for each sample and element.

| Sample Name | $\Gamma_i$ [×$10^{23}$ $\text{m}^{-2}\,\text{s}^{-1}$] | $\lambda_{\text{MFP}}$ [mm] | $\Delta m_{loss}^e$ [mg] | $\Delta m_{loss}^m$ [mg] | $\Delta m_{gain,N}^m$ [µg] | $\Delta m_{gain}^e$ [µg/cm$^2$] | $\Delta m_{gain}^m$ [µg/cm$^2$] | $R_{loss}$, % | $R_{gain}$, % |
|---|---|---|---|---|---|---|---|---|---|
| **Cu 1** | 0.3 | 45.4 | 15.6 | 4.28 | 1.3 | 17.6 | 3.49 | **72.6** | **80.2** |
| | | | ±9.4 | ±0.07 | ±0.1 | ±10.9 | ±0.04 | -42.4/+10.6 | -33.2/+7.7 |
| **Cu 2** | 1.1 | 18.7 | 67 | 3.01 | 120 | 76 | 1.50 | **95.3** | **98.0** |
| | | | ±34 | ±0.05 | ±10 | ±39 | ±0.02 | -5.0/+1.6 | -2.1/+0.7 |
| **Cu 3** | 5.7 | 4.2 | 170 | 0.41 | 870 | 194 | 0.57 | **99.3** | **99.7** |
| | | | ±90 | ±0.05 | ±10 | ±98 | ±0.01 | -0.8/+0.3 | -0.3/+0.1 |
| **Cu 4** | 8.5 | 2.8 | 360 | -0.81 | 1020 | 410 | 0.88 | **99.94** | **99.8** |
| | | | ±180 | ±0.03 | ±80 | ±209 | ±0.01 | -0.11/+0.04 | -0.2/+0.1 |
| **Cu 6** | 1.7 | 12.4 | 33 | 0.68 | 16 | 37 | 0.43 | **97.9** | **98.8** |
| | | | ±17 | ±0.03 | ±1 | ±19 | ±0.01 | -2.3/+0.8 | -1.2/+0.4 |
| **Cu 8 (He)** | 1.7 | 50.8 | 13.0 | 0.29 | 72 | 14.7 | 0.27 | **95.3** | **98.0** |
| | | | ±6.5 | ±0.04 | ±6 | ±7.5 | ±0.01 | -2.9/+1.0 | -2.1/+0.7 |
| **Mo 1** | 0.3 | 56.1 | 0.58 | 0.58 | 1.3 | 0.7 | 1.4 | - | - |
| | | | ±0.58 | ±0.06 | ±0.1* | ±0.7 | ±0.01 | | |
| **Sn 1** | 0.3 | 61.2 | 11.0 | 1.52 | 1.3 | 12.4 | 0.68 | **86.2** | **94.5** |
| | | | ±5.5 | ±0.05 | ±0.1* | ±6.2 | ±0.01 | -14.4/+4.8 | -5.7/+1.9 |
| **Sn 2** | 1.7 | 16.5 | 22.8 | 0.41 | 16.3 | 25.8 | 0.18 | **98.1** | **99.3** |
| | | | ±13.7 | ±0.03 | ±1.3* | ±15.6 | ±0.01 | -3.0/+0.8 | -1.2/+0.3 |

**Table 2: Summary of the determined measured and expected mass losses and mass gains and the derived re-deposition rates, as well as the mean free path of the target material in each case.**
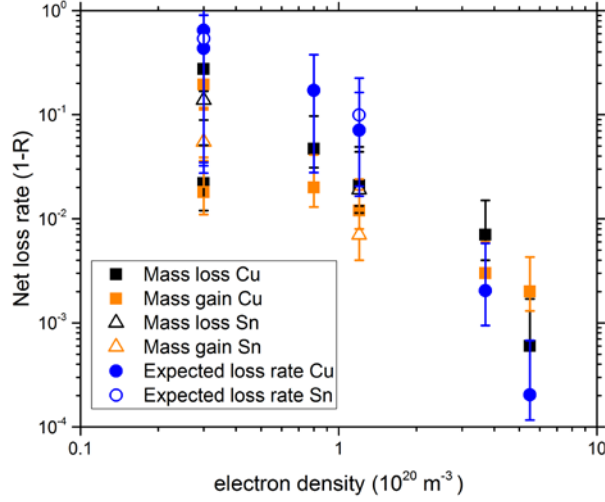


**Figure 11: The net loss rate (1-*R*) of the sputtered element as a function of electron density. The expected losses are calculated using equation (5).**

Data in Table 2 show very consistent re-deposition ratio between the sample mass loss and the mass gain on the QCM. This gives high confidence in the results given such highly similar values by two different methods. One can see a clear growth of re-deposition ratio with increasing flux of incoming ions and simultaneous decrease of the mean free path as the density increases.

One can also describe the expected net loss rate (i.e. $1 - R$) as the fraction of particles which escape collisions, such that

$$1 - R = \exp\left(-\frac{L_{plasma}}{\lambda_{MFP}}\right). \tag{5}$$

Where we define the characteristic scale of the plasma ($L_{plasma}$) as the FWHM of the plasma beam as given in table 1. These expected losses are shown in comparison to the measured data in Figure 11, indicating relatively good agreement given the uncertainties in defining both $L_{plasma}$ and $\lambda_{MFP}$ and confirms that the processes of momentum and charge exchange identified are sufficient to account for such high re-deposition ratios. This is also in qualitative agreement with the OES observations as the ratio of impurity line intensities at the target relative to at the TS position 3 cm upstream increases with flux. In other words as the density increases, at the position of the TS an increasing fraction of the sputtered particles are no longer present and are presumably entrained and redeposited relative to what is spectroscopically observed at the target. When this path length becomes smaller than the characteristic plasma size (in the Magnum-PSI case approximately 2-4 cm) then re-deposition becomes very strong.

We can now also consider the implications for ITER and DEMO. In SOLPS-type codes ion-neutral friction between the plasma and impurities is typically not considered, as both the friction and thermal forces are generally only concerned with charged-species collisions [34][35][36]. However, when electron temperatures are sufficiently low, sputtered neutrals can have relatively long lifetimes and should not be neglected. Analogous to the friction force for ions, the friction force for ion-neutral friction can be derived as

$$F_{in}^0 = m_z(v_i - v_n)/\tau_{in}^{mt} \tag{6}$$

Where $\tau_{in}^{mt} \approx (n_i v_i \sigma^{mt})^{-1}$ is the collision time for momentum exchange under the assumption that $v_i \gg v_n$. However, unlike for ion-impurity and electron impurity collisions for charged particles (*z*) which have a

dependence $\tau_{ez}^{mt} \propto T_e^{3/2}$ and $\tau_{iz}^{mt} \propto T_i^{3/2}$ respectively, thus giving rise to the electron temperature and ion temperature gradient thermal forces, it follows from equation (3) that $\tau_{in}^{mt}$ is independent of $T_i$, and therefore ion-neutral collisions are not subject to thermal forces. As this force is that which typically directs particles away from the surface and towards the main plasma this indicates that in regions where ion-neutral collisions are important entrainment by friction will be the dominant force leading to efficient re-deposition at the wall. It can also be noted that cross sections for the momentum and charge exchange cross-sections do not vary strongly when hydrogen isotopes or helium are chosen rather than argon as the ion species. Taking as an example a partially detached DEMO scenario calculated using SONIC gives ion density of $2\times10^{20}$-$2\times10^{21}$ m$^{-3}$ with electron temperatures in the range 1-5 eV in the detached region. In the 1-2 cm inside the attached region the ion temperature reaches ~100 eV while the ion density drops to ~$2\times10^{19}$ m$^{-3}$ [37]. For a W-based divertor this would give re-deposition rates above 99.9% in the detached region at the highest densities but this rapidly becomes unimportant ($R$~5%) in the 1-2 cm region just outside this if we assume that the characteristic plasma dimension ($L_{plasma}$) is given by the ionization mean free path (~1 mm) [37]. Predominantly this is due to the strongly decreasing $L_{plasma}$ and $n_i$, for cases where ionization mean free paths are longer re-deposition processes will be more important. As most sputtering is expected to take place in the attached region ion neutral friction is therefore unlikely to be of significance for the erosion lifetime of the strikepoint region of a W divertor except for sputtered neutrals which enter the detachment region and potentially during transient events such as ELMs. However, for liquid metal divertors the region of highest evaporation is likely to be at the detached strikepoint locations where the heat load is highest. (1-$R$) can easily reach <$10^{-4}$ in such a case, assuming a conservative ionization mean free path in this case of ~1 cm. If $L_{plasma}$ is of order the poloidal width of the detached region (~10 cm) then (1-$R$)→0. Such very high re-deposition rates imply that the operational temperature for liquid metals may be significantly extended upwards compared to estimates neglecting such re-deposition processes [2].

## 7. Conclusion

Re-deposition of Cu, Mo and Sn was studied under high-flux Ar (0.3-8.5$\times10^{23}$ m$^{-2}$s$^{-1}$) and He (1.7$\times10^{23}$ m$^{-2}$s$^{-1}$) plasma exposure. Mass loss and QCM measurements showed consistent results between the measured mass loss rate of the samples and the mass gain rate on the crystal. XPS demonstrated a radial distribution of re-deposited particles, rising to the edge of a sample. RBS analysis was used to determine the deposited Mo mass on the sample surface and take this into account for the re-deposition calculation. We observed a strong dependence of re-deposition ratio on the plasma flux and particle density. Plasma entrainment of sputtered particles is considered to be the primary process for such high re-deposition ratios. The effect does not appear to depend strongly on particle or target species, but is strongly correlated with the mean free path of the particles, which for the entrainment process is inversely proportional to $n_i$. This dependence appears to agree well with the results (figure 11). The maximum re-deposition rate is estimated at ~99.8% at the highest flux based on the more conservative of the two measurement approaches. These measurements and calculations are consistent with our previous work [8], where a highly sensitive absorption technique Cavity-Ring-Down-Spectroscopy was used to measure the re-deposition ratio of tin. It should be noted, that while these experiments were predominantly carried out in Ar, cross-sections of similar magnitude would be expected for plasma entrainment for such materials with hydrogen isotope ions or other species. The results agree reasonably well with the expression $1 - R = \exp(L_{plasma}/\lambda_{MFP})$ which indicates re-deposition rates above 99.99% should be possible at the high density regions of the DEMO divertor. This is positive for all materials but in particular, this can increase operating temperatures limited by evaporation for liquid metals used at the divertor strikepoints of DEMO.

**Bibliography**

[1] Kleyn A W, Lopes Cardozo N J and Samm U 2006 Plasma–surface interaction in the context of ITER Phys. Chem. Chem. Phys. 8 1761–1774

[2] Morgan T W, Rindt P, van Eden G G, Kvon V, Jaworski M A and Lopes Cardozo N J 2018 Liquid metals as a divertor plasma facing material explored using the Pilot-PSI and Magnum-PSI linear devices Plasma Phys. Control. Fusion 60 014025

[3] Fetzer R, Igitkhanov Y and Bazylev B 2015 Efficiency of water coolant for DEMO divertor Fusion Eng and Design 98–99 1290–93

[4] You J H et al. 2015 Conceptual design studies for the European DEMO divertor: Rationale and first results Fusion Eng. Des. http://dx.doi.org/10.1016/j.fusengdes.2015.11.012

[5] Maisonnier D et al. 2007 Power plant conceptual studies in Europe Nucl. Fusion 47 1524–1532

[6] van Rooij G J et al 2007 Extreme hydrogen plasma densities achieved in a linear plasma generator App. Phys. Let.90 121501-3

[7] Abrams T, Jaworski M, Chen M, Carter E, Kaita R, Morgan T W, Stotler D, De Temmerman G, van den Berg M A and van der Meiden H J 2016 Suppressed gross erosion of high-temperature lithium via rapid deuterium implantation Nucl. Fusion 56 016022

[8] Kvon V, Al R, Bystrov K, Peeters F J J, van de Sanden M C M and Morgan T W 2017 Tin re-deposition and erosion measured by Cavity-Ring-Down-Spectroscopy under a high flux plasma beam Nuclear Fusion Vol 57 Nr 8 DOI: https://doi.org/10.1088/1741-4326/aa79c4

[9] van Eden G G, Kvon V, van de Sanden M C M and Morgan T W 2017 Oscillatory vapour shielding of liquid metal walls in nuclear fusion devices Nature Communications 8, Article number: 192 doi:10.1038/s41467-017-00288-y

[10] H.J.N. van Eck, T.A.R. Hansen, A.W. Kleyn, H.J. van der Meiden, D.C. Schram and P.A. Zeijlmans van Emmichoven 2011 Plasma Sources Scienceand Technology 20, 045016

[11] H.J.N. van Eck et al., 2007 Fusion Eng. Design 82 1878

[12] H.J.N. van Eck, A.W. Kleyn, A. Lof, H.J. van der Meiden, G.J. van Rooij, J. Scholten and P.A. Zeijlmans van Emmichoven 2012 Applied Physics Letters 101, 224107

[13] Morgan T W, Vertkov A, Bystrov K, Lyublinski I, Genuit J W and Mazzitelli G 2016 Power handling of a liquid-metal based CPS structure under high steady-state heat and particle fluxes Nucl. Mater. Energy 10+ (2017) in press

[14] Coenen J W, De Temmerman G, Federici G, Philipps V, Sergienko G, Strohmayer G, Terra A, Unterberg B, Wegener T and van den Bekerom D C M 2014 Liquid metals as alternative solution for the power exhaust of future fusion devices: status and perspective Phys. Scr. T159 014037

[15] Stangeby P C 2000 The Plasma Boundary of Magnetic Fusion Devices (ISBN: 0-7503-0559-2 Bristol, UK) p 647

[16] van der Meiden H J et al 2008 High sensitivity imaging Thomson scattering for low temperature plasma Rev. Sci.Instrum. 79 013505

[17] Scofield J H 1976 Hartree-Slater subshell photoionization cross-sections at 1254 and 1487 eV Journal of Electron Spectroscopy and Related Phenomena Vol. 8, 129-137

[18] Alcock C B, V P Itkin, and Horrigan M K 1984 Vapor pressure of the metallic elements Canadian Metallurgical Quarterly 23 309

[19]    Behrisch R and Eckstein W 2007 ed C E Ascheron Sputtering by Particle Bombardment Experiments and Computer Calculations from Threshold to MeV Energies (Topics in Applied Physics) Vol 110ISBN: 978-3-540-44502-9 (Berlin: Springer) p 509

[20]    Sauerbrey G 1959 Verwendung von Schwingquarzen zur Wägung dünner Schichten und zur Mikrowägung Zeitschrift für Physik 155 (2): 206–222,doi:10.1007/BF01337937

[21]    QCM100 – Quartz Crystal Microbalance Theory and Calibration, Stanford Research Systems

[22]    Irem Tanyeli I, Laurent Marot L, van de Sanden M C M, and De Temmerman G 2014 Nanostructuring of Iron Surfaces by Low-Energy Helium Ions Appl. Mater. Interfaces, 6 (5), pp 3462–3468 DOI: 10.1021/am405624v

[23]    Sansonetti J E and Martin W C 2005 NIST: Handbook of Basic Atomic Spectroscopic Data American Institute of Physics (J. Phys. Chem. Ref. Data) Vol. 34 No. 4 DOI: 10.1063/1.1800011

[24]    Mott N F and Massey H S W The theory of atomic collisions 1965 (UK, Oxford University press) p 643

[25]    Deutsch H, Becker K and Mark T D 2008 Calculated absolute cross-sections for the electron-impact ionization of atoms with atomic numbers between 20 and 56 using the Deutsch-Mark (DM) formalism International Journal of Mass Spectrometry 271 58–62

[26]    Bartlett P L and Stelbovics A T 2002 Calculation of electron-impact total-ionization cross sections Physical Review A 66, 012707

[27]    Margreiter D, Deutsch H and Mark T D 1994 A semiclassical approach to the calculation of electron impact ionization cross-sections of atoms:from hydrogen to uranium International Journal of Mass Spectrometry Vol. 139 Nr. Pag. 127-139

[28]    Freund R S, Wetzel R C, Shul R J, and Hayes T R 1990 Cross-section measurements for electron-impact ionization of atoms Physical review A vol. 41, Number 7 1

[29]    Wolfgang L 1970 Electron-Impact Ionization Cross-sections for Atoms up to Z=108* Zeitschrift Physik Vol. 232 101-107

[30]    Kudriavtsev Y, Villegas A, Godines A and Asomoza R 2005 Calculation of the surface binding energy for ion sputtered particles *Applied Surface Science* Volume 239, Issues 3–4, Pages 273–278

[31]    Banks P 1966 Collision frequencies and energy transfer Planet. Space Sci. Vol. 14. 1105-1122

[32]    Teachout R R and Pack R T 1971 The static dipole polarizabilities of all the neutral atoms in their ground states Atomic data 3 195-214

[33]    Hutchinson I H Principles of plasma diagnostic 2002 2nd ed (ISBN 0 521 80389 6, UK, Cambridge, Cambridge University press) p 347

[34]    Sytova E, Kaveeva E, Rozhansky V, Senichenkov I, Voskoboynikov S, Coster D, Bonnin X and Pitts R A 2018 Impact of a new general form of friction and thermal forces on SOLPS-ITER modelling results Contributions to Plasma Physics  https://doi.org/10.1002/ctpp.201700135

[35]    Takizuka T and Abe H 1977 A binary collision model for plasma simulation with a particle code Journal of Computational Physics Vol. 25 Issue 3 205-219

[36]    Homma Y and Hatayama A 2013 Numerical modeling of the thermal force in a plasma for test-ion transport simulation based on a Monte Carlo Binary Collision Model (II) – Thermal forces due to temperature gradients parallel and perpendicular to the magnetic field Journal of Computational Physics Vol. 250 206-223

[37]    Homma Y et al. 2017 Numerical analysis of tungsten erosion and deposition processes under a DEMO divertor plasma Nuclear Materials and Energy Vol. 12 323-328